IDENTIFICATION AND CHARACTERIZATION OF THE WING REFERENCE AREA OF BLENDED WING BODY AIRCRAFT FOR ASPECT RATIO DEFINITION

Schneider J.[1], Blessing S.[1], Zander J.[1], Strohmayer A.[1]

Abstract

The Blended-Wing-Body (BWB) aircraft concept has gained significant attention in recent years due to its potential for increased fuel efficiency, reduced noise levels and increased fuel capacity which is a critical driver for hydrogen powered aircraft. However, the lack of a standardized design methods for BWB aircraft has led to confusion and inconsistency in performance analyses. One of the challenges in the preliminary design of BWB aircraft is the definition and configuration of the wing reference area, which is critical for determining important design parameters such as the wing loading and performance parameters such as the lift- and drag coefficients.

This study presents an aerodynamic analysis of a BWB aircraft based on panel methods focusing on defining the reference area for preliminary aircraft sizing. The fundamental concept is to exactly identify and quantify the wing area responsible for generating a positive lift force with a Python based procedure developed for this purpose. The aerodynamic analysis involved varying the angle of attack, Mach number, Reynolds number and the BWB configuration itself to investigate the aerodynamic characteristics of the aircraft. In an additional study, the blended section, as the significantly different part from conventional aircraft, has been investigated in detail regarding the influence of relevant geometric parameters.

From the simulated data, a simple numeric and alternatively a geometric method has been derived to facilitate the use of the wing reference area definition in preliminary aircraft design tools such as UNICADO[2] with sufficient accuracy and to have a comprehensive method for the definition of the wing reference area of BWB aircraft.

The proposed method to identify and specify the wing reference area of BWB aircraft leads to more accurate predictions of aerodynamic performance and provides a consistent basis for comparison between BWB aircraft designs and conventional aircraft. Moreover, the method can serve as a useful baseline for future BWB aircraft design and optimization studies.

In addition, the studies carried out on the blended section are bridging the gap between theoretical aerodynamic findings and practical design considerations, by formulating a concrete preliminary design approach for the blended section of fuselage and wing for BWB aircraft. Covering these aspects, this work provides a valuable contribution to the development of BWB aircraft design and sizing methodologies, and highlights the potential benefits of this configuration.

Keywords: conceptual aircraft design · initial aircraft sizing · Blended-Wing-Body · UNICADO

Acknowledgements

The funding of this investigation, which was done within the LuFo VI-2 project UNICADO-II, by the *Bundesministerium für Wirtschaft und Klimaschutz* is gratefully acknowledged.

✉ Johannes Schneider
Johannes.schneider@ifb.uni-stuttgart.de

[1] Institute of Aircraft Design, University of Stuttgart, Germany
[2] University Conceptual Aircraft Design and Optimization Software

Abbreviations

BWB	Blended-Wing-Body Aircraft
TLAR	Top Level Aircraft Requirement
TAW	Tube and Wing

1. Introduction

The Clean Sky Development Plan [5] emphasizes that politics and society are focusing on the limitation of climate change. Every industry has to reduce their emissions and environmental impact. Although aviation has continuously improved fuel efficiency, its growth is overtaking those advances. "Currently, the aviation sector is responsible for about 12% of transport emissions and 2% of all human-induced CO2 emissions [...]" [5]. The ambitious goals of the Advisory Council for Aviation Research and Innovation in Europe from 2017 is to achieve "[...] a 75% reduction in CO2 emissions, a 90% reduction in NOX and 65% reduction in perceived noise by 2050 compared to year 2000 levels [...]" [5, 8].

Since the introduction of the Boeing B-47 Stratojet [30] in 1947, there has been a steady evolution of the tube-and-wing airliner with podded engines mounted below the swept wings [17]. The concept has seen a tremendous success, with all modern long range airliners resembling the B-47. However, unconventional aircraft configurations can help to leverage synergy effects of different new technologies further increasing the energy efficiency and thus to achieve the emission goals.

The Blended-Wing-Body (BWB) aircraft is a proposal that utilizes advantages of a new aircraft configuration, but is held back by not only the higher development cost by deviating from the proven tube-and wing design, but also by stability and control issues [4]. First concepts of the related flying-wing aircraft had already been envisioned in the 1910's with the first operational prototypes being developed during the 1940's in Germany by the Horton brothers and in the US by Northrop [16]. The advent of fly-by-wire technology and digital flight control systems enabled flying-wing aircraft such as the Northrop-B2 [20].

First studies on the BWB show potential in takeoff mass reduction up to 15% and fuel savings of more than 25% [16, 17]. Moreover, with an increase in air travel, the issue of noise pollution is becoming more prevalent. BWB aircraft also possess a lower acoustic signature than traditional tube-and-wing aircraft [21, 29].

McDonnell Douglas started research on the BWB in the early 1990's under the X-48 program [16]. From 1997 onward, successful flight tests were performed with scaled flight test beds, [15] validating the BWB concept. A full size, piloted BWB is yet to be tested. Nonetheless, the concept is recently gaining momentum in academia and the aerospace industry.

Initial sizing of an aircraft uses simplified methods to estimate the performance of a design to verify that the demands formulated as the Top Level Aircraft Requirements (TLARs) are fulfilled. With only a small number of parameters, these methods must be accurate enough to result in an aircraft concept with the desired performance.

In preliminary aircraft design, reference values and calibration are used to validate methods and fundamental aircraft parameters and performance. Since the BWB configuration is unprecedented in civil aviation, no reference parameters exist. The University Conceptual Aircraft Design and Optimization (UNICADO) project aims to establish a collaborative academic aircraft preliminary design software. Consequently, it includes a database of aircraft reference configurations [23]. To enable the development of BWB aircraft within the UNICADO framework, establishing generic methods and guidelines are essential [26].

2. Objective

The goal of this work is to develop a method for determining a meaningful wing reference area (S_{ref}) of a BWB aircraft which can be applied in the preliminary design phase. The method shall enable the aircraft designer to determine S_{ref} in a simple and short procedure as is the case with common procedures for conventional configurations. The value of S_{ref} shall represent the actual area of a BWB

aircraft responsible for generating lift in the design point. This is to ensure consistency between the determined aerodynamic coefficients and the actual aerodynamic performance of the aircraft. Moreover, in terms of aircraft sizing processes, less iterations are necessary if the reference area matches the physical behavior of the geometry. Otherwise, transferring the results from aerodynamic analysis of the design back into the sizing loop needs to be transformed.

In this work, the wing reference area is theoretically determined with numerical simulations of four selected aircraft models and subsequently transferred in a method applicable for various BWB configurations.

In terms of the investigation of the blended part, this work is centered around the manipulation of parameters found in wing design, which define the geometry of the blended section and can be considered part of the lift-generating geometry. A variation of these parameters therefore alters the reference area of the aircraft.

The insights learned from these evaluations are then extrapolated to a preliminary aircraft design method by formulating guidelines for the design approach of the blended section. In addition, the influence of wing parameter changes on fundamental characteristics in preliminary aircraft design, such as the wing area, are evaluated.

3. Background and state of art

The term BWB denotes configurations between conventional Tube and Wing (TAW) and flying wing designs. As can be seen in Figure 1, this configuration is characterized by a blending of the fuselage and the wing. It also dispenses with a tail. A similar term in the United States for the BWB configuration is "hybrid wing body" [18]. Although investigated since decades, there has never been a BWB aircraft in airline service. Therefore, there is not yet an established standard configuration.

The basic idea of the BWB concept is to minimize the wetted area (S_{wet}) of an aircraft and therefore maximize the lift to drag ratio (L/D) [22]. The most radical way to achieve this goal leads to the so-called flying wing [18].

Figure 1: Airbus ZEROe BWB concept [1]

Both, the BWB and the flying wing, have an airfoil shape for the longitudinal cross section,

The BWB aircraft needs to be highly integrated, incorporating the landing gear and control surfaces and in some cases the propulsion system within the airfoil shape [16]. The configuration possesses stability and control challenges just as tailless aircraft. Other challenges include the pressurized passenger compartment. As the hull is not cylindrical, the hoop-tensile strength of a traditional tube-and wing configuration is not present [16].

The differences in the initial sizing of conventional TAW and unconventional BWB aircraft are examined in [31]. It is investigated whether the established methods to size a conventional aircraft can also be used to size a BWB aircraft. While most of the relations can be used similarly or with modified coefficients, S_{ref} can not be determined in the same way as it is generally done for conventional configurations. This relies on the fact, that the center body of a BWB and its airfoil shape generates a significant amount of lift [3]. In [31] it is stated, that the methods applied to a BWB configuration "[...] generally result(s) in a bigger reference wing area than TAW aircraft" [31]. In order to create a sizing chart for a BWB it is assumed S_{ref} to equal the whole planform of the aircraft projected on the top view. However, it is to be expected that its actual size will be smaller. Due to the smooth transition, the wing size and “fuselage” size of

a BWB cannot be determined isolated like for a TAW aircraft because it is not clearly separated anymore [6]. However, the wing size is one of the parameters getting changed the most in a preliminary aircraft design iteration loop.

Liebeck investigated the differences between the TAW and BWB design in terms of weight. He assumed the center body of a BWB to be manufactured with composites whereas the wings are made of aluminum. A total reduction of approximately 15% in takeoff weight has been predicted [17].

The engine integration which is often envisaged on top of the aft section of the BWB allows for shielding the soundwaves from the engines in the downward direction [32]. Additionally, the centerbody shields forward radiated fan nose, and engine exhaust noise is not reflected from the lower surface of the wing. Airframe noise is reduced by the absence of a slotted flap trailing-edge high-lift system [14].

The BWB configuration has more volume available in the centerbody compared to the TAW design. This additional volume is located in the blended area between the center body and the wing. Additional volume is located around the multiple cylindrical sections used inside the centerbody for the cabin. Therefore the BWB shows a lot of potential in combination with liquid hydrogen (LH2) as fuel which needs approximately three times the volume of kerosene to store the same amount of energy [11]. Additionally, LH2 needs to be stored at temperatures of about −253°C and pressurized [12]. To provide the optimal environmental conditions for this fuel, spherical or cylindrical tanks are needed [2], difficult to place inside a conventional aircraft. The cylindrical fuselage has to be extended or the space available for payload has to be reduced in order to place the cylindrical tanks inside the fuselage. This increase in fuselage volume in order to only store fuel is not needed for a BWB due to a larger available volume in the body.

The wing reference area is a design parameter used to characterize the size of an aircraft's wing. It is used in conjunction with other factors, such as airspeed, to calculate aerodynamic force- and moment coefficients such as lift- and drag coefficients. Therefore, it provides a convenient way to compare and analyze the aerodynamic performance of different aircraft, regardless of their specific wing configurations and size. In initial aircraft sizing, the wing reference area is one of the most important parameters to modify, as it ultimately is a lever for the adjustment of the performance of an aircraft in several ways such as takeoff, climb and landing performance along with the maneuverability of the aircraft in the design and sizing process.

Looking at TAW aircraft, S_{ref} is defined to extend through the fuselage and is therefore a fictitious area and not a physical one [24].
The additional wing area in the center section serves to compensate the contribution of empennage and fuselage to the aircraft's aerodynamics. Therefore, it represents the area which matches the aerodynamic capabilities and performance of the aircraft. However, there are several definitions and methods how to specify S_{ref}, according to different aircraft manufacturer.

A visualization of these different methods is given in Figure 2. They do have in common that they describe a projected area based on the top view. Further, all of them cover at least the planform area of the wing. They differ in the definition of the fuselage area. one of the methods connects the wing roots horizontally (cf. Figure 2 (a)). Another company practiced a method, where the wing's leading- and trailing edge sweep is extended with its half magnitude (cf. Figure 2 (b)). A third method works similar to the latter with the difference, that the wing sweep is extended with its original magnitude (cf. Figure 2 (c)).

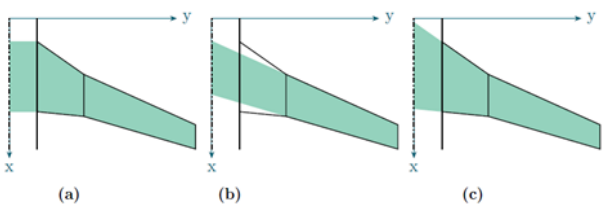

Figure 2: Different wing reference area definitions. Own illustration based on [28]

As mentioned before, it is expected that the BWB fuselage part generates a significant amount of lift because of the geometry and airfoil which is applied to the centerbody.

Therefore, it is highly doubtful that the established methods determine a suitable wing reference area for the BWB configuration which is consistent with the aerodynamic properties of the aircraft.

4. Approach, models and tools

Firstly, a set of different BWB configurations has been developed based on existing concepts. This is due to the lack of a standardized BWB aircraft configuration. Investigating different BWB configurations serves to find more generic and robust methods.

All four models shown in Figure 3, named Model A,B,C,D, are created with *OpenVSP* [13], . a parametric aircraft geometry tool. OpenVSP allows the user to create a 3D model of an aircraft defined by common engineering parameters. This model can be processed into formats suitable for engineering analysis [13]. The BWB Models only consist of a single wing body structure each and are further specified section-wise. All models consist of a centerbody, the blended section and the outer wing (cf. Figure 19). The centerbody of all models is section 1. It has the same root chord and span for all models and is designed to carry the same amount of passengers (Figure 4). The passengers are sitting in separated pressurized tubes within the BWB shape, sized according to conventional aircraft fuselage standards and methods.

In Model A and Model B the blended part consists of three sections and the outer wing consists of one section. Model C and Model D have a blended part of only one section and an outer wing of two sections.

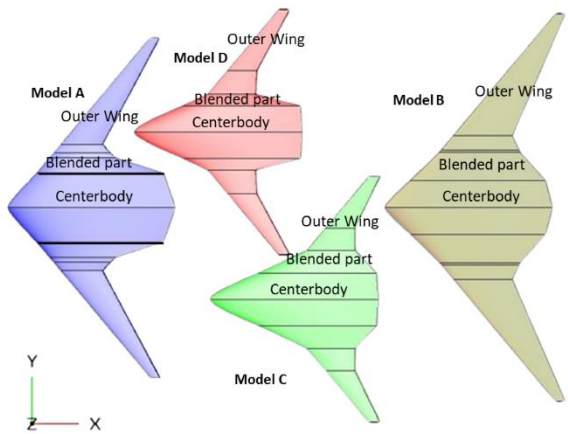

Figure 3: Investigated Blended Wing Body Configuration

Models A and B and Models C and D are pairs of rather similar configuration. The main difference between the two pairs is the leading edge. Models A and B have a constant leading edge sweep and therefore no kinks in the leading edge. Further, the geometrically determined aspect ratio is higher for Model A and B (5.7 and 5.9) than for Model C and D (3.9 and 4.3). The pairs itself differ from each other mainly in the span of the blended section only.

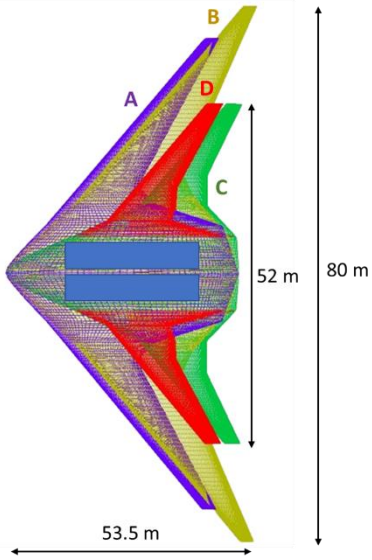

Figure 4: Overlay of investigated BWB configurations

For the centerbody, the symmetrical NACA 0016 airfoil is used for all Models. Symmetrical Airfoils offer the most space to include the passenger tubes within the airfoil. Furthermore the moment coefficient is relatively low which helps to maintain pitch stability without a proper vertical tailplane. In Models A and B, the first section of the blended part uses the NACA0014 symmetrical airfoil, the second

section of the blended part the airfoil is aerodynamically twisted from the NACA0014 to the supercritical NASA SC(2)-0712 airfoil. The third section of the blended part and the outer wing are equipped with the same supercritical airfoil. In Models C and D, the blended section aerodynamically twists from the symmetrical airfoil at the root to the before mentioned supercritical airfoil at the tip of this section. Source files of the airfoils have been downloaded from UIUC Airfoil Database [27].

The BWB models are transformed into a surface mesh for the aerodynamic investigation with the software *FlightStream®,* a surface vorticity flow solver which employs a panel method but also considers compressibility effects and flow separation [25]. This tool allows fast investigation and comparison of different models, configurations of the blended section and environmental conditions which cannot be obtained from Computational Fluid Dynamics (CFD) simulations in a reasonable timeframe. Moreover, the fidelity level of the tool is sufficient since the lift is the main parameter to analyze from the results for the reference area investigation.

For the blended section, the effects of different wing geometry parameters on the aerodynamic performance are evaluated in a separate investigation. This is achieved by analyzing the distribution of lift and lift-coefficient, the lift-to-drag ratio, pressure-distribution and cumulative lift force generated.

To efficiently obtain usable data and decrease the number of parameter variations, a two-step approach is utilized. At first the focus lies on the chord length and the wing span of the blended section, since those parameters have the most significant impact on the planform shape of the aircraft. This is due to both the cord length and the wing span majorly altering the size of the wing. In the second step, the wing sweep and wing twist are varied once satisfying values have been found for the chord length and wing span. In the next step, the influence of the varied chord length and wing span on the wing area, taper ratio and aspect ratio is shown. With the gained insight, an optimized model is created on which the wing sweep and wing twist are examined.

The analysis of the results from FlightStream are done in Python and Matlab as well as the corresponding visualizations. Additionally, the FlightStream results have to be processed in advance of the analysis. This step is also done with a Python code. Both codes are written in the Python version 3.9.13.

4.1 Results analyzing method

In the following the methods for evaluation and visualization of the simulation results are explained. In general, the analysis involves the detection of aerodynamic forces along an arbitrary body in a flow. Those aerodynamic forces are pressure forces which means that they act perpendicular to the surface. Figure 5 shows the cross section of an exemplary wing airfoil as well as a schematic pressure-force-distribution around it.

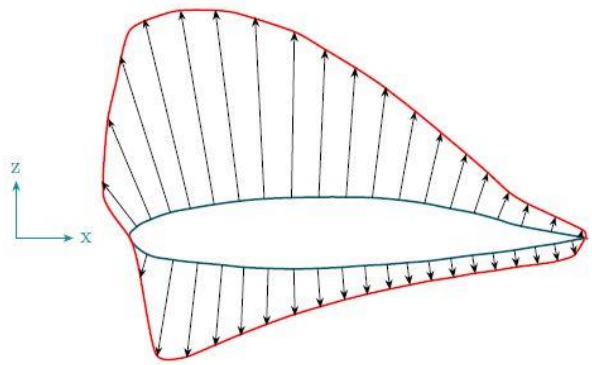

Figure 5: Pressure-distribution of an airfoil

The solver of FlightStream® delivers the acting aerodynamic force at every node of the mesh. It stores the force separated by its spatial components Fx, Fy and Fz. As can be seen in Figure 6 the total force at each node is composed of those partial forces according to the spatial directions. The main interest for the analysis lies on Fz because this component denotes the lift force.

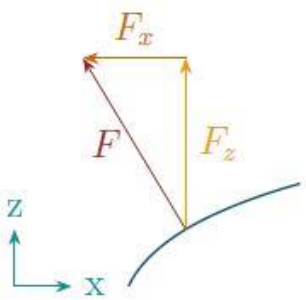

Figure 6: Vector composition of airfoil forces

The goal of this analysis method is to determine the proportion of an aircraft's area which is responsible for generating lift. This is achieved by summing the pressure forces of the upper and lower side including the position information of the force in the aircrafts coordinate system. Only the force components in the Z-direction are summed and rooted to the xy-plane. This means the local Fz of the upper side is summed up with the local Fz from the underside of the wing which is directly on the opposite side, resulting in a force Fz in the xy plane at a designated position on the wing which is either positive or negative and therefore this designated area is contributing to the total lift or not. The concept of this procedure is outlined in Figure 7.

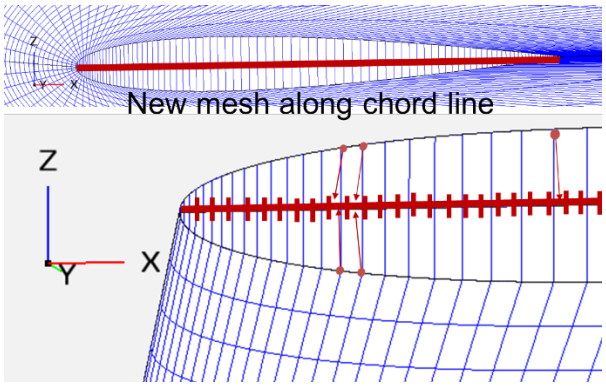

Figure 7: Mapping concept of upper and lower surface forces in a new mesh

As mentioned in the section before, this mapping is done with a python script and in two steps as follows.

Step 1: The projected area of the aircraft from its top view is separated into a set number of cells for its length (x-axis) and its width/span (y-axis). In spanwise direction an equal cell distribution is implemented and a hyperbolic tangent-type clustering for the x-axis. This special distribution allows a higher density of the mesh at the leading and trailing edge of the body where the highest deviations between neighbor cells is expected. The individual cell height according to the distribution is given in the form

$$\Delta x_i = \left(1 + \frac{\tanh(s) * z}{\tanh(s)} * \frac{1}{2} * l\right) with\ z = \frac{2i - n}{n}$$

i is the index of the current cell. n denotes the number of cells. l is the total length of the cells that are distributed, which equals the chord length of the designated spanwise position. The distribution of the cells in x-direction can be controlled with the stretch s [9]. Figure 8 shows different cell distributions for $0.6 \leq s \leq 1.4$. The direct comparison shows that at a stretch of less than 1 the level of detail of the edges is weak. With a stretch of 1.4, on the other hand, the cells in the middle area are fairly large to be able to reproduce fine differences accurately enough. Therefore, for this work, the stretch is set to 1.2, since the emphasis is clearly on the edge cells, but the middle cells should not be too stretched.

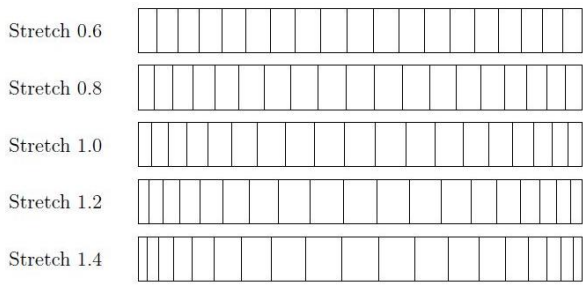

Figure 8: Cell distribution with different stretches

A mesh with 30 cells in x-direction with a stretch of 1.2 and 20 cells in y-direction is illustrated as an example for Model A in Figure 9. The hyperbolic cell distribution in x-direction is performed separately for every y-section as can be seen in the figure below (Figure 9).

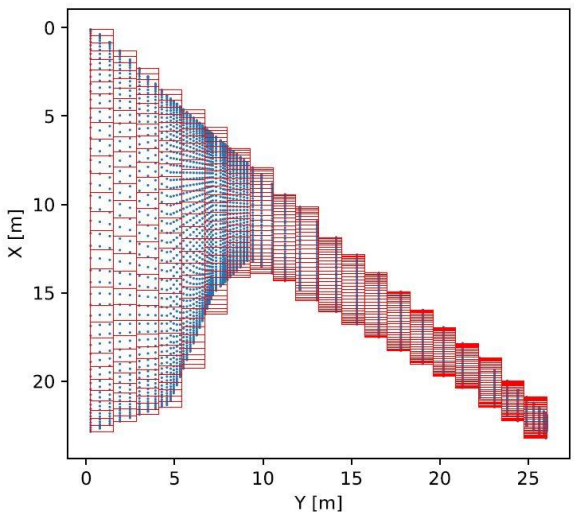

Figure 9: Analysis mesh for the lift area determination (Model A)

Figure 10 shows a part of the outer wing section. The contour of the projected aircraft area is illustrated with black lines. It is visible, that the mesh area does not exactly match the projected wing area. However, this error does not affect the calculated amount of lift as it does not change the number of Fz vectors from the simulation results that are rooted from the upper and lower surface and summed up in the corresponding cells of the new mesh, nor change their magnitude. The total mesh area is also expected to approximately equal the projected area.

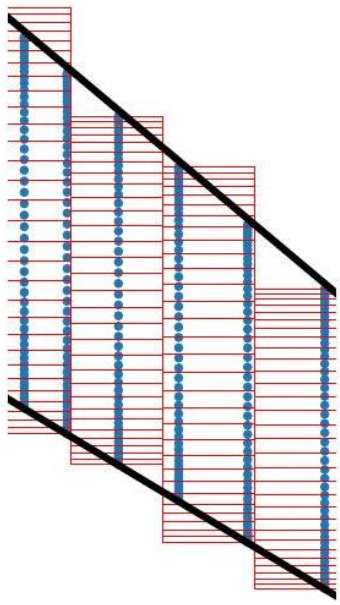

Figure 10: Deviation from mesh area from aircraft shape

On the one hand the total mesh area is slightly larger at the leading and trailing edge of the mesh. On the other hand it does not cover the area between the points with the minimal y-coordinates and the symmetry plane (y = 0). This relies on the fact, that the cell distribution is performed within the minimal and the maximal values for the x and y-coordinates of the data points. A print command in the analysis code allows the determination of the mesh area. A comparison of the mesh area of the models with the planform area given by OpenVSP, which is the projected area in the xy-plane, shows a minimum difference of +1.46% (Model B) to a maximum of +2.46% (Model A). In order to have a python script for the mesh generation and analysis as generic as possible and usable for many different BWB shapes, the accuracy and size of the analysis mesh compared to the actual wing shape and size has been considered sufficient. Additional refinement functions in the code for the leading and trailing edge would be dependent and individual for each BWB geometry to analyze.

In the following analysis, the ratio of total mesh area to mesh area with positive lift is investigated.

In FlightStream the aircraft mesh is fixed to the coordinate system and not rotated for angle of attack (AoA) investigations. Instead the free stream air flow is rotated with the AoA variations. Therefore, no further deviations as shown in Figure 11 of the projected area to the xy-plane occur in different AoA simulations.

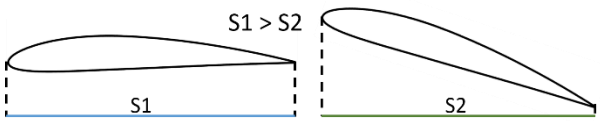

Figure 11: Deviation of projected area due to AoA

Step 2: The sum of the lift forces of all nodes within each cell of the analyzing mesh is calculated. The cells will be colored depending on their resulting lift force. However, it shall be noted that the simulation takes advantage of the aircrafts symmetry and only calculates the flow of a half span model to save computing time.

5. Reference Area Investigation Results

In order to compare the results of all four BWB models, the setup and the environmental conditions have not been changed. All simulations have been done with a constant freestream at a Mach number of 0.82 at 36000ft cruise altitude and the corresponding atmospheric data from the U.S. Standard Atmosphere [19], see Model C as an example (Figure 12). Furthermore, a transitional turbulent viscous boundary layer is regarded in the investigations. The handling of viscous coupling is enabled as well as flow separation, whereas the surface roughness height is set to zero by default

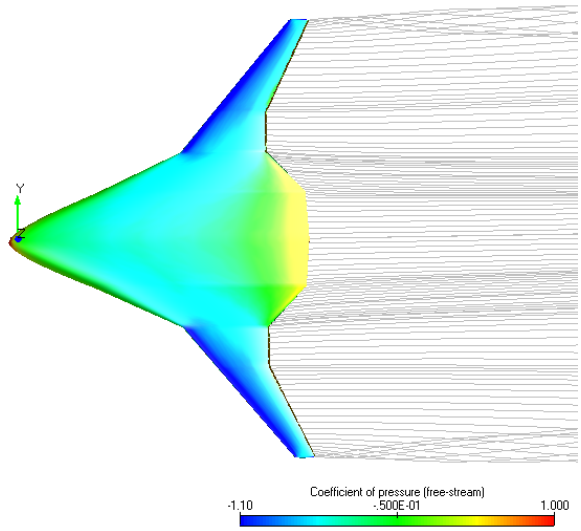

Figure 12: Pressure-coefficient-distribution from FlightStream

The equation for the total lift force

$$L = \bar{q} * S_{ref} * C_L$$

shows that the lift coefficient C_L is the only variable for the calculated lift as long as the altitude and the cruise speed - and therefore the dynamic pressure - remain constant. C_L depends on the AoA. It is therefore the only entity which is varied during the simulations. A typical range of the AoA for the cruise flight is from -3° to +3°. In the simulations for this work, the AoA is varied from -5° to +20° to investigate the whole flight envelope for changes of the lift relevant area in dependence of the AoA.

The results of the various AoA simulations are visualized with the method described in Section 4.1. Figure 13, Figure 14, Figure 15 and Figure 16 show the plot for all four models at an AoA of 0°.

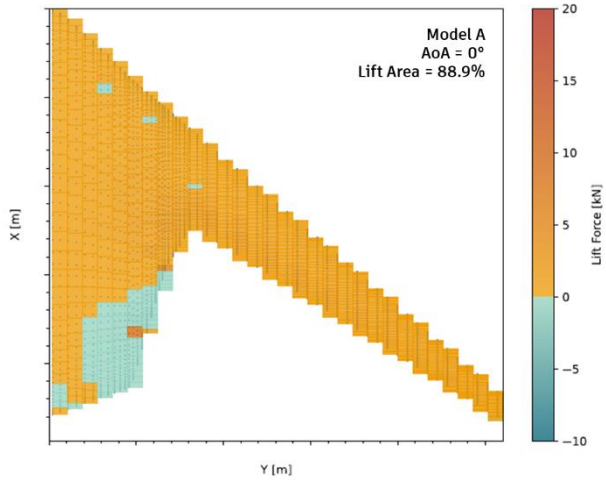

Figure 13: Lift-force-distribution plot Model A

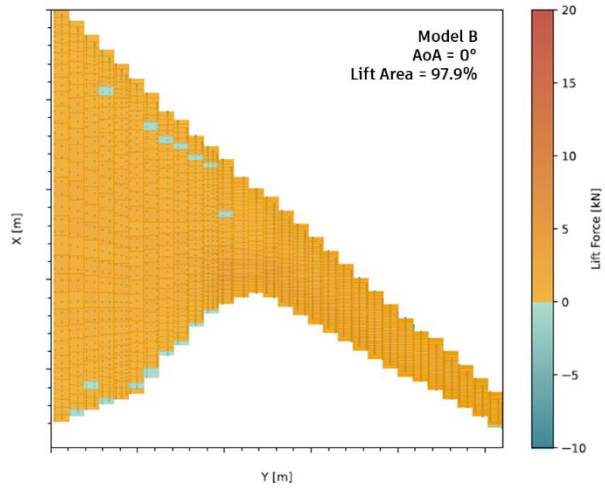

Figure 14: Lift-force-distribution plot Model B

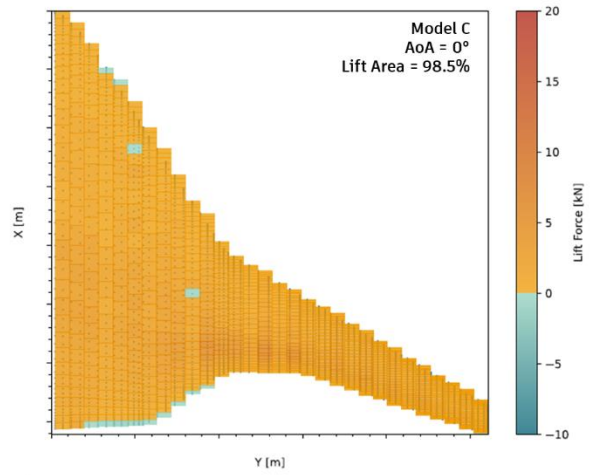

Figure 15: Lift-force-distribution plot Model C

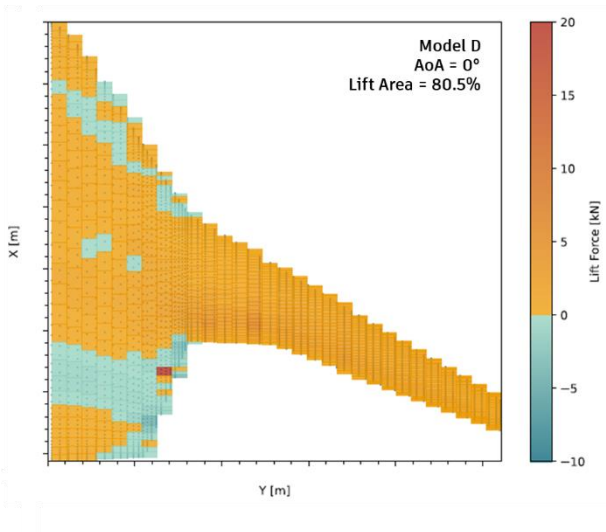

Figure 16: Lift-force-distribution plot Model D

For the Models A and B, most of the cells in the shown lift-distributions do have a lift force in the range of −1 and +5 kN. Model C and D do have a slightly higher lift density in the blended part. These commonalities are not surprising, as Model B is a modification of Model A and Model D is a modification of Model C. Apart from their differences in shape, Model B and Model C have a similar uniform distribution of lift force. The same is true for Model A and Model D, where for both the lift force is partially negative at the rear of the centerbody. The explanation for this connection can be seen in the commonality of the models A & D and B & C, respectively. Models A and D have a fairly high sweeped trailing edge at the blended part and therefore a sharp transition to the outer wing, while models B and C show a smoother transition in the blended part.

From this visual investigation it can be concluded that the entities associated with the blended part of the wing are influencing the ratio of the lifting area and the geometric planform area.

In the investigation of the influence of the blended part of a BWB aircraft on its lift coefficient distribution, total lift, and liftdistribution, described in section 6, these results have been used as a constraint for the different blended part configurations analyzed. Regarding the AoA variation, further influence on the lift area ratio has been found. Especially negative AoAs result in a significant loss of aerodynamically lifting surface area (Figure 17, Figure 18). This is due to the design of the centerbody with its symmetrical airfoil.

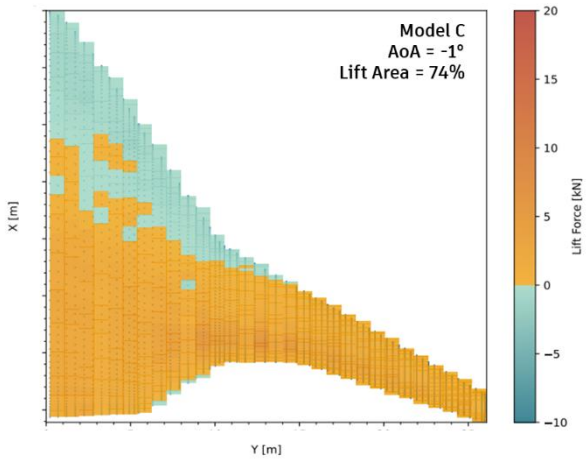

Figure 17: Lift-force-distribution plot Model C at -3° AoA

For all models it has been found that increasing AoAs lead to slightly less lifting surface and therefore to a decreasing lift area ratio. The combined results of all four models over the total AoA envelope from -5° to 20° is shown in Figure 18.

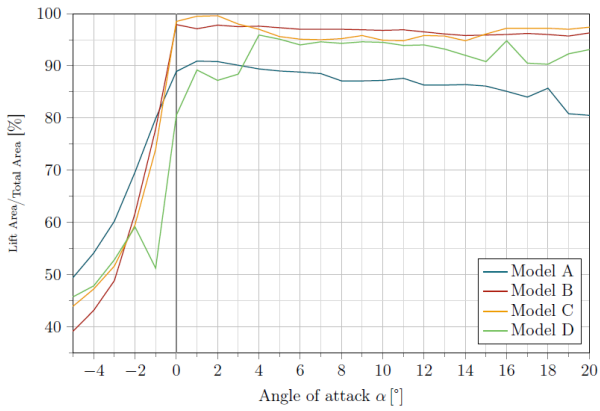

Figure 18: Ratio of lift area/total area for AoA variation

6. Investigation of blended section

The composition of the chord lengths, the span and the sweep angle of the blended section have the most impact on the planform shape and wing area of the aircraft. Therefore, an investigation of the geometry of the blended part has been conducted.

The aerodynamic properties are examined by analyzing the lift-distribution and lift-coefficient-distribution. For the lift-distribution the evaluation criteria is, how closely it matches an ideal elliptical lift-distribution. The lift-coefficient-distribution is evaluated on the location of the maximum lift coefficient $C_{L,max}$. With respect to the stall characteristics it is beneficial, when $C_{L,max}$ is located closer to the wing root than to the wing tip. Additionally, a

higher lift coefficient is considered more advantageous than a lower value.
A secondary criteria for both distributions is, how steady the plots are. Sudden changes in the distributions usually coincide with abrupt changes in the geometry, which can increase turbulence and increase the induced drag. The pressure distribution is visually evaluated. Unusual behavior, such as spikes in pressure towards the trailing edge of the wing, are investigated and can lead to mesh optimizations.
To determine the range over which the parameters chord and span should be varied, a visual approach is utilized. The condition for the chord length is, that going from the middle of the aircraft to the wingtip, the chord length always has to decrease. This avoids any geometry with spikes protruding from the trailing edge of the aircraft.
For the following investigation, identifiers are introduced as defined in Figure 19 to characterize different parts of the blended section. The Root-Chord-Length (RC) corresponds to the chord length at the transition of the centerbody to the blended part. The Mid-Chord-Length (MC) is only applicable for Model A and B and corresponds to the chord length at the airfoil twist section. The Tip-Chord-Length (TC) corresponds to the chord length at the transition to the outer wing. The wing span identifier (SP) refers to the span of the blended section.

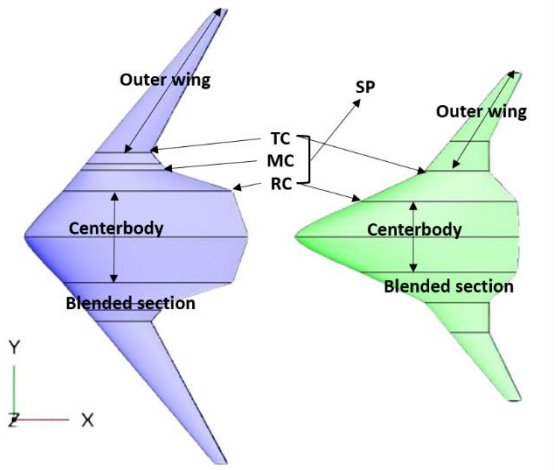

Figure 19: Definition of blended section identifiers

In the plots for the lift- and lift-coefficient-distribution, the vertical blue lines represent the location of the blended part. The deviation value, displayed in the lift-distribution plot's legend, indicates how closely the lift-distributions matches an elliptical-lift-distribution. It is determined by the difference in area under the elliptical-distribution and the simulated lift-distribution. This approach was chosen to consider changes to the entire distribution in order to evaluate it quantitatively. For example, a maximum vertical distance between the simulated and ideal distribution does not take into account changes to the overall distribution. A lower deviation value therefore indicates a distribution matching the elliptical-distribution more closely. The ideal elliptical-distributions, which change for each geometric modification, are indicated by the light green area, as plotting the calculated individual equation would make the plot confusing.

Aerodynamic investigation of chord lengths and span of blended section

The figure below (Figure 20) shows the results of varying the tip chord of the blended section.

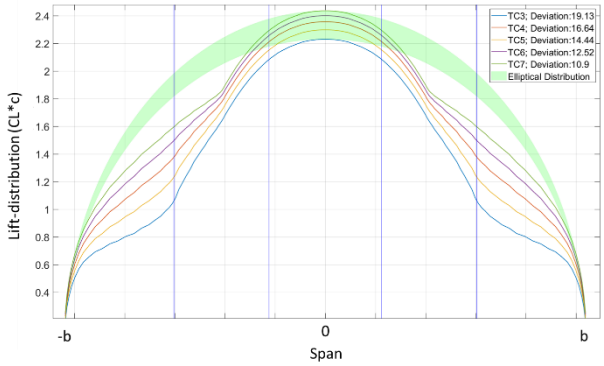

Figure 20: Spanwise lift-distribution with variable blended-section-tip-chord

Changing the TC value results in the most significant change to the lift-distribution. This is indicated by a 43% change in the deviation value between the lowest and the maximum value for TC which has been applied in the investigations. The maximum tested TC value delivers the best result in terms of lift-distribution.

The lift-coefficient-distribution (Figure 21) does not follow the same principle as the lift-distribution. A high TC value results in $C_{L,max}$ being located near the tip of the wing. Very short TC values result in a spike in the lift-coefficient-distribution. Both extremes are undesirable, therefore a medium tip-cord should be selected to achieve good-natured stall behavior.

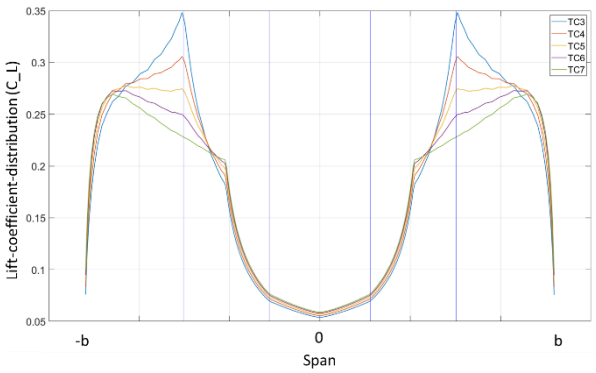

Figure 21: Lift-coefficient-distribution with variable TC

Regarding the lift-distribution, a change in wing span is largely negligible, as the deviation value only changes in a range of 1% to 6% between the smaller and larger wing spans of the investigated blended part. However, the largest SP still delivers the lift-distribution closest to the elliptical lift-distribution. The lift-coefficient-distribution changes in a way, that a smaller value for SP results in a higher C_L value close to the center body. However, the spanwise location of $C_{L,max}$ is not affected by changes of the SP value.

Following the same principle as for the chord length variation, the span of the blended section has been investigated. The lift-distribution of the wing is shown in Figure 22.

It can be concluded, that a change in span is largely negligible, as the deviation value only changes in a range of 1% between the highest and lowest investigated span. However, the maximum SP value possesses the most ideal lift-distribution, with the distribution matching the elliptical distribution 6% more closely than the shortest investigated span for the blended section.

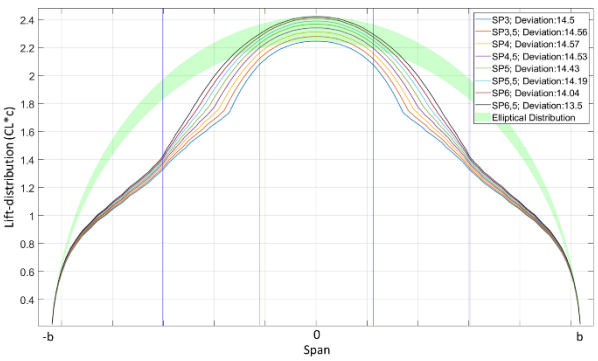

Figure 22: Lift-distribution with variable SP

The effects of a changing wing sweep angle has also been evaluated. It can be stated that the wing sweep angle has little impact on the lift-distribution and lift-coefficient-distribution. A higher wing sweep angle results in a slightly more elliptical lift-distribution, meanwhile the lift-coefficient-distribution result in slightly lower C_L values in the center of the blended section and the outer wing. The position of $C_{L,max}$ however, is unaffected.

Lift-to-drag ratio investigation

Furthermore, the same identifiers (RC, MC, TC & SP) are used to investigate the influence of chord length and wing span alterations on the lift-to-drag ratio. It has been determined, that with a decreasing RC value, the lift-to-drag ratio increases. In a +-30% parameter variation of RC from a baseline model, the lift-to-drag ratio decreases approximately linearly by 13% from the smallest RC to the largest RC. This investigation coincides, since the lift- and lift- coefficient-distribution both also improve with a decreasing RC. For a MC variation of +-50% from a baseline, the difference between the highest and lowest tested lift-to-drag-ratio is 5%. The impact of a changing MC value is therefore noticeably less significant than changing the RC value.

In contrast to the previous results, increasing the TC value also increases the lift-to-drag ratio. The impact of changing the TC value is therefore higher than changing the MC value, but less significant than the impact of the RC value. The lift-distribution has also been found superior for larger TC values.

Influence of chord lengths on the wing area

As changes to the chord length and wing span result in a significant alteration of the geometry, the influence on the wing area is examined. Figure 23 shows the influence of the chord lengths TC and MC on the wing area.

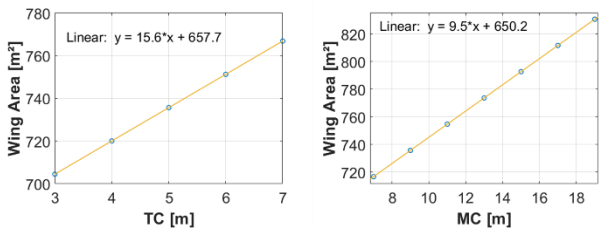

Figure 23: Change of wing area with varying chord lengths TC and MC

The equation, which describes the dependency between chord, span and area is also shown in the diagrams. This is achieved by fitting a function to the data points. This allows for a general statement about the influence of each parameter on the wing area. Increasing the chord length, increases the wing area linearly. Figure 24 shows the influence of the chord lengths RC and the span of the blended section on the wing area.

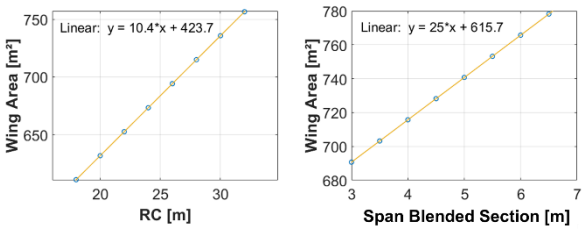

Figure 24: Change of wing area with varying chord length RC and span of the Blended Section

By examining the constants of the equations, the influence of changing RC, MC and TC values can be compared. The TC value has the most influence on the wing area, with a constant of 15,6. In other words, changing the chord length in the outermost part of the blended section has the most impact on the wing area of the BWB. Changing the chord length in the middle (MC) or towards the centerbody (RC) of the blended section, has less impact on the wing area. This is indicated by the smaller constants in the equations.

Increasing the wingspan of the blended section also increases the wing area linearly (Figure 24). The constant describing the linear dependency is 25. A direct comparison to the chord length's influence has reservations, as different parameters are being varied. However, changing the wing span of the blended area by a given percentage has a larger impact on the wing area, than changing the chord length by the same percentage.

Investigation in context of the aspect ratio

The results from the lift-to-drag ratio analysis are reexamined in the context of the aspect ratio. The aspect ratio is an important parameter in preliminary aircraft design, as it links the wing span and wing area and has a profound impact on the aerodynamic properties of a wing [10]. A high aspect ratio results in less induced drag being generated. Additionally, high CL values are achieved, when increasing the aspect ratio. The wing span of the BWB models are constrained to either 52m or 80m by TLARs. With decreasing chord length values, the wing area decreases, as shown in Figure 23 and Figure 24. As a result the aspect ratio steadily increases.

For changes to RC and MC value, the convention, that a higher aspect ratio results in a higher lift-to-drag ratio holds true. When decreasing the TC value, however, the aspect ratio increases but the lift-to-drag ratio decreases. This is likely due to the complex geometry of the blended area, which does not resemble the comparatively simple trapezoidal wing planform, for which the convention holds true. The aspect ratio in its current definition can therefore not be considered a reliable parameter in predicting lift-coefficient, induced drag and lift-to-drag ratio of BWB configurations.

7. Application of study results in initial BWB aircraft sizing

In this section the results of the aerodynamic analysis of the reference wing area and the blended section shall be transformed in applicable initial BWB sizing methods. In terms of the wing reference area, a method shall be derived which delivers the wing reference area of a wide range of BWB planform geometries, respecting the behavior found for lift-area ratios. Therefore, the reference area used in the further sizing respects the actual lifting area of the aircraft. In order to make the method applicable for a wide range of planforms and easy to use, a minimal amount of variables shall be used. Since the section chord and section spans are the main driver for the aerodynamic behavior, a model shall be found to replicate the lift area ratios of the BWB Models identified in this work.

A numerical method to determine the lift area ratio

The aim of the numerical approach is to correlate geometric characteristics of the BWB planform with the actual lift area. Several attempts to find a ratio of sections chord and width result in a pairwise similar number of pairwise similar models. E.g. the product of the

ratios of the chord c of two neighbored sections (Sn) and the ratio of the centerbody-span (b) and the blended section-span gives for Model A:

$$\frac{C_{S1}}{C_{S0}} * \frac{C_{S3}}{C_{S2}} * \frac{C_{S5}}{C_{S4}} * \frac{b_{S2}}{b_{S4}}$$

$$= \frac{17.4m}{23m} * \frac{7.8m}{9m} * \frac{1.4m}{5.4m} * \frac{6.7m}{8.2m} = 0.1389$$

A random exponent combined with cosine allows this exemplary chord-span-relation to get in a closer range of the desired lift area ratio:

$$\cos(0.1389^{0.5)} = 0.9314$$

The same equation for Model B delivers a value of 0.9326. These numbers are |93.12% − 87.0%| = 6.12% and |93, 26% − 96.7%| = 3.44%, respectively, off the identified ratios. The different chord ratios in this equation could be adjusted with exponents to fit the desired ratios. However, the main problem with the chord and span ratios persists. Models A and B should differ in about |96.7 %−87.0%| = 9.7% which is not the case in any tried variation of the chord and span ratios. Same is valid for Model C and D. They do only have five sections and therefore the section relations of Section 1 and 0 and Section 3 and 2 are used with the same principle as shown in the suggested cosine equation above. It provides the value 0.8534 for Model C and 0.8689 for Model D. Their actual difference is |86.89%−85.34%| = 1.55%. Again, the numbers are similar for the rather similar Models C and D. They should, however, differ by |96.5% − 92.1%| = 4.4%.

Inspecting the models' top views in Figure 2 is revealing another possibility to determine the average lift-area-ratios with aircraft proportions. In terms of the leading edge, Model C and D and Model A and B are similar. The course of the lift area ratios over the AoA from Figure 18, however, looks more similar for Model B and C and for Model A and D, although, at first glance they look geometrically rather different. Except for the trailing edge of the blended part, where both models have a high trailing edge sweep angle and therefore a sharp transition between the centerbody and the wing. Model A and D do have a similar, rather smooth transition between the centerbody and the wing, regarding the trailing edge.

The trailing edge angle appears to be a unit that can be used for a simplified method to determine the lift-area ratio and therefore the reference area of a BWB. The goal is to determine a "smootheness factor" which replicates the lift area ratio of the models. A simple multiplication with the total planform area of the aircraft would allow to get the reference wing area.

The trailing edge angles of all sections can be read out of the top view. Model A is shown as an example in Figure 25 and in Table 1.

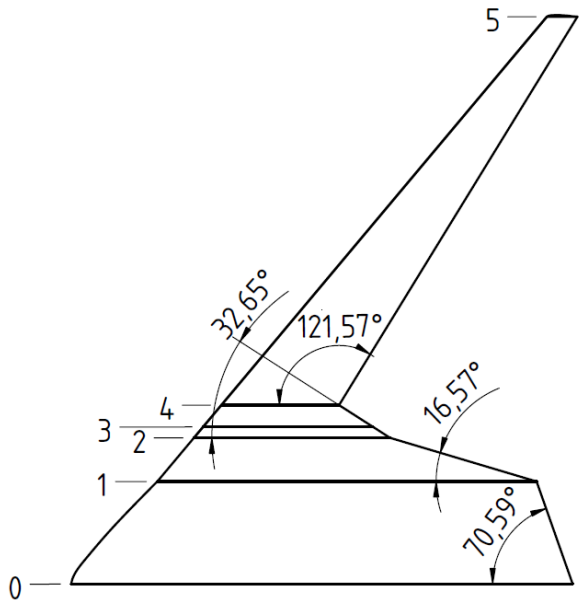

Figure 25: Top-view Model A with sweep angles

All angles are measured parallel to the X axis. However, the wing sweep is by definition measured to the Y axis. Subtracting the illustrated angles from 90° results in the trailing edge wing sweep. One goal of the method is to minimize the number of used variables. This can be achieved by not considering the trailing edge angle of every single section, but to consider them all at once. The average trailing edge sweep of the centerbody (CB) & blended part (BP) is calculated for each model and listed in Table 1 .

Table 1: Section wise trailing edge sweep angles

Section	Model A	Model B	Model C	Model D
S0 to S1	-19.41°	-19.41°	-4.13°	-4.13°
S1 to S2	-73.43°	-45.78°	-43.19°	-75.16°
S2 to S3	-57.35°	-29.29°	0.53°	3.39°
S3 to S4	-57.35°	-17.79°	25.73°	28.26°
S4 to S5	31.57°	28.78°	-	-
CB&BP	-51.86°	-28.07°	-15.60°	-25.30°

The sweep angle given below is the arithmetic mean of the angles between Section 0 and Section 4 in Models A and B and between Section 0 and Section 3 in Models C and D. The average trailing edge sweep combines all other angles into one. Its cosine allows to map the angles to a number between zero and one, while not preserving their sign. The lower the angle, the higher the cosine of it and vice versa. With this calculation the small sweep angles, which correspond to a soft transition, receive a higher score than the large angles, which correspond to a hard transition. This behavior is also visible in the average lift area ratios of the models. The cosine of the average CB&BP sweep angles is

$\cos(-51.86°) = 0.617$ for Model A

$\cos(-28.07°) = 0.882$ for Model B

$\cos(-15.60°) = 0.963$ for Model C

$\cos(-25.30°) = 0.904$ for Model D.

The ranking highest to lowest BWB Model is: C > D > B > A, which is not exactly as desired comparing it to the ranking of Figure 18 which is for a cruise AoA of 1,5° C > B > A > D. However, adding an exponent to the cosine scales the numbers closer to the range of the average lift area ratios. After applying several numbers between 0 and 5 as the exponent, the closest results can be achieved with the exponent $1/3$ which leads to the formula:

$$\sigma = \cos(\varphi_{TE,CB\&BP})^{\frac{1}{3}}$$

This results in a predicted lift area ratio of 0.851 for Model A, 0.959 for Model B, 0.988 for Model C, and 0.967 for Model D.

These numbers match within a satisfying 2% range for Model A and B, but not for Model C and D. In the following the leading edge sweep for Models C and D shall also be considered. Again, the difference of the leading edge sweeps between the CB and the outer wing is used.

The average CB sweep of Model C and D is $\frac{61.29°+65°}{2} = 63.15°$. Both Models have an outer wing sweep of 40°. Therefore the sweep difference of CB and outer wing is $63.15° - 40° = 23.15°$. The cosine of the difference in the angles again allows to emphasis smaller differences. In other words, a higher weighing factor for smoother transitions. Since Model A and B have no sweep difference they get the factor $\cos(0°) = 1$. For Model C and D the factor is $\cos(23.15°) = 0.92$. The closest results for the lift area ratio again can be achieved with an exponent of $1/3$.

This leads to the modified formula for the smoothness factor which also respects the leading edge:

$$\sigma = \cos(\varphi_{TE,CB\&BP})^{\frac{1}{3}} * \cos(\varphi_{LE,CB} - \varphi_{LE,W})^{\frac{1}{3}}$$

With this formula the lift area ratio of all 4 investigated BWB models can be determined within a range of 1.9%.

Simplification of the numerical method

The trailing edge sweep can be easily read out of a model or drawing made with computer-aided design programs. This method however aims to determine the reference area during the initial design of a BWB aircraft. This design phase is characterized by iterative methods, which typically involve multiple changes to the models [7]. In case no automated tool is available, determining the section wise leading- and trailing edge sweeps is inaccurate and time consuming. Therefore, the method is to be modified further, to enable the goal of a simple procedure that can also be done by hand.

Unifying the section (cf. Figure 26 orange lines) of the center body and the blended part into a single trapeze makes measurements quicker and more accurate.

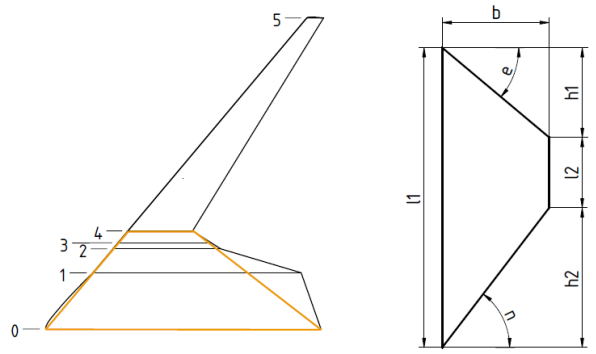

Figure 26: Top view of Model A with substitute trapezoid and definition of properties

The leading edge sweep e and the chord lengths $l1$ and $l2$ are assumed to be the given entities. $h1$ and $h2$ are supporting lengths. They are related to the sweep angle by its tangent.

$$\mathrm{h1} = \mathrm{b} * \tan e \ ; \ \mathrm{h2} = \mathrm{b} * \tan e$$

With this, the trailing edge sweep n can be derived: $n = \arctan\left(\frac{l1-l2}{b} - \tan e\right)$.

Finally, the prior introduced formula for the lift area ratio determination can be modified to:

$$\sigma = \cos(\varphi_{TE,CB\&BP})^{\frac{1}{3.8}} * \cos(\varphi_{LE,CB\&BP})^{\frac{1}{1.75}}$$

where $\varphi_{TE,CB\&BP}$ is n and $\varphi_{LE,CB\&BP}$ is e

Testing this formula with all four BWB models gives a satisfaying accuracy of the lift area ratio, where the deviations are in a range of +1.5%. Furthermore, the BWB design simplifies significantly to a double trapezoidal wing form. This allows the usage of well-known formulas and relations for other aerodynamical design aspects.

Design guidelines for the initial sizing of the blended part

With the insight gained in from the detailed blended section investigations, a methodology for the preliminary design and sizing of the centerbody-wing transition in BWB aircraft shall be derived. The aspect ratio, taper ratio and wing area all serve as performance indicators in preliminary aircraft design, as they allow to predict aerodynamic performance without describing the exact geometry of the wing.

However, when applying the aspect ratio and taper ratio to the blended area, no reliable prediction about the aerodynamic performance of the BWB can be made. In order to reliably predict the influence of the CB-wing transition's geometry, the following parameters have to be considered individually.

The lift- and lift-coefficient-distributions of the whole BWB aircraft are greatly influenced by the chord length of the blended section. The impact on the distributions increases, the further away from the center body the chord length is changed.

The location of $C_{L,max}$ is determined by the chord length at the tip of the blended area, which corresponds to the root of the outer wing. An optimal lift-to-drag ratio is present for the chord length in the middle of the blended area. A larger wing span results in a smoother transition of CB-outer wing and a larger wing area. The wing span can also be used to tweak characteristics of the lift- and lift coefficient distribution, however, the overall impact of the wing span has been found to be smaller than other criteria.

8. Summary and Outlook

A comprehensive investigation of BWB aircraft has been conducted. Changing different wing parameters of the blended section between the centerbody and the outer wing has a varying degree of influence on the aerodynamic properties.

At first, suitable models for investigation were developed. In first aerodynamic studies with the software OpenVSPaero, the influence of the sectional chord and span on the lift-distribution and lift-coefficient-distribution has been analyzed.

The chord length influences the lift-distribution differently, depending on how far away from the centerbody the change occurs. A change in chord length at the tip of the blended section has the most significant impact on the shape of the lift-distribution of the whole wing. The lift coefficient-distribution is influenced locally by changes to the chord length at the respective

location. A lower chord length generally results in a higher section lift-coefficient. The location of the maximum section lift-coefficient is influenced mainly by changes to the chord length at the tip of the blended section. Changes in the wing span or wing sweep of the blended section have less influence on the lift-coefficient-distribution.

In order to develop a methodology to determine the wing reference area, four different BWB configurations from the blended section investigation have been analyzed further with the commercial software FlightStream®. The flow solver results are analyzed using a Python code developed specifically for this purpose. The code identifies the locations on the wing where lift is generated. Although the Models A and B as a pair and the Models C and D are rather similarly shaped, the results of Models B and C are more similar to each other. Models A and D show less similarity in results. The driving factor for this phenomenon is identified as the smoothness of the transition from the centerbody to the outer wing. Models B and C have a similar smooth transition, whereas Models A and D have a sharp transition. Throughout the whole range of AoA analysis, all models have an area of 87% to 96.7% of the total planform area which can be considered as aerodynamically relevant to be the wing reference area. The larger lift area ratio belongs to the models with a smoother transition. Negative lift is mostly generated at the aft centerbody of all models.

A numeric method is carried out to determine the ratio of the planform area that is responsible for generating lift. This method uses the trailing edge sweep of a substitute trapezoid, which supersedes the centerbody and the blended part of the BWB. A cosine relation is found to estimate the lift area ratio. The determined ratio of the numerical method differs by a maximum of 1.3% from the average lift area ratios determined with the simulation data.

Outlook

The derived methods are based on aerodynamic studies with vorticity flow solvers. Although a BWB aircraft in terms of flow simulations is a relatively less complex task, the simulated aerodynamic data should be validated in a future study by utilizing a CFD simulation tool, or in a practical approach conducting wind tunnel tests with the analyzed models. Furthermore, the methods determined are not analytically derived, but empirically determined. Therefore, they cannot be considered as generally valid for all BWB configurations. They can be applied to BWB aircraft similar in shape to the four models studied. Future research could cover the analysis of numerous additional BWB configurations that have a wide variety in their geometry parameters, to empirically extend the validity of the developed methods.

To refine the analysis method, there are also improvements that can be made subsequently to this work. The Python code which is used to analyze the 3D-lift-distribution and forces, only uses rectangles as mesh elements. This causes the calculated mesh area to deviate from the actual planform area of the aircraft. Changing the mesh elements to triangles can replicate the planform area more accurately.

This change only needs to be done to the first (leading edge) and the last (trailing edge) mesh element in every section. However, the improvement is not expected to be significant. The current deviation of the net area to the planform area is at about 2.5%. It would also not change the number of force vectors used for the investigation and therefore not change the calculated lift. Currently, the Python code uses the same amount of cells in every section. The sections, however, have different chord lengths. This causes the wing sections to be divided into tiny cells compared to the center body sections. Using a variable number of cells in X-axis direction could help to keep the cells in a similar size spanwise.

References

[1] Airbus. *ZEROe. Towards the world's first hydrogen-powered commercial aircraft*. https://www.airbus.com/en/innovation/low-carbon-aviation/hydrogen/zeroe. Accessed 2 December 2023.

[2] Airbus. 2021. *How to store liquid hydrogen for zero-emission flight*. https://www.airbus.com/en/newsroom/news/2021-12-how-to-store-liquid-hydrogen-for-zero-emission-flight. Accessed 4 December 2023.

[3] Bil, C., Cho, S., and Adams, R. 09212011. Design and Analysis of BWB Military Cargo Centre Body Structure. In *AIAA Centennial of Naval Aviation Forum "100 Years of Achievement and Progress"*. American Institute of Aeronautics and Astronautics, Reston, Virigina. DOI=10.2514/6.2011-7026.

[4] Bradley, K. R. 2004. *A Sizing Methodology for the Conceptual Design of Blended-Wing-Body Transports* NASA/CR-2004-213016, Hampton, VA, USA.

[5] Clean Sky 2 Joint Undertaking. 2021. *Developement Plan*. https://www.clean-aviation.eu/sites/default/files/2022-03/CS2DP-October-2021.pdf. Accessed 1 December 2023.

[6] Dorsey, A. and Uranga, A. 08022021. Design Space Exploration of Blended Wing Bodies. In *AIAA AVIATION 2021 FORUM*. American Institute of Aeronautics and Astronautics, Reston, Virginia. DOI=10.2514/6.2021-2422.

[7] Fielding, J. P. 2017. *Introduction to aircraft design*. Cambridge University press, New York.

[8] Ganesh kumar Badri narayan. 2018. *How to create a non-uniform 2d grid*. Matlab Community. https://de.mathworks.com/matlabcentral/answers/378693-how-to-create-a-non-uniform-2d-grid. Accessed 29 January 2024.

[9] Gudmunsson, S. 2022. *General Aviation Aircraft Design*. *Applied Methods and Procedures*. Butterworth-Heinemann; Elsevier, Oxford.

[10] Hoelzen, J., Silberhorn, D., Zill, T., Bensmann, B., and Hanke-Rauschenbach, R. 2022. Hydrogen-powered aviation and its reliance on green hydrogen infrastructure – Review and research gaps. *International Journal of Hydrogen Energy* 47, 5, 3108–3130.

[11] Institut für Luft- und Kältetechnik gemeinnützige Gesellschaft mbH. *Wasserstoff- und Methan-Versuchsfeld am ILK*. https://www.ilkdresden.de/leistungen/forschung-und-entwicklung/. Accessed 4 December 2023.

[12] J.R. Gloudemans. 2012. *OpenVSP*. National Aeronautics and Space Administration.

[13] Kozek, M. and Schirrer, A., Eds. 2014. *Modeling and Control for a Blended Wing Body Aircraft*. *A Case Study*. Advances in Industrial Control. Springer.

[14] Kroo, I. The Effect of Aircraft Size on Performance. Aircraft Aerodynamics and Design group, Department of Aeronautics and Astronautics 1995.

[15] Larrimer, B. I. [2020]. *Beyond tube-and-wing*. *The X-48 blended wing-body and NASA's quest to reshape future transport aircraft*. NASA aeronautics book series NASA-SP-2020-644. USA, Washington, DC.

[16] Liebeck, R., Page, M., and Rawdon, B. 01121998. Blended-wing-body subsonic commercial transport. In *36th AIAA Aerospace Sciences Meeting and Exhibit*. American Institute of Aeronautics and Astronautics, Reston, Virigina. DOI=10.2514/6.1998-438.

[17] Liebeck, R. H. 2004. Design of the Blended Wing Body Subsonic Transport. *Journal of Aircraft* 41, 1, 10–25.

[18] National Oceanic and Atmosperic Administration. 2021. *The U.S Standard Atmosphere, 1976*. *NOAA-S/T 76-1562*. Also filed as NASA TM X-74335. https://www.ngdc.noaa.gov/stp/space-weather/online-publications/miscellaneous/us-standard-atmosphere-1976/us-standard-atmosphere_st76-1562_noaa.pdf. Accessed 30 January 2024.

[19] Northrop Grumman. *B-2 Spirit Stealth Bomber*. https://www.northropgrumman.com/what-we-do/air/b-2-stealth-bomber. Accessed 1 December 2023.

[20] Okonkwo, P. and Smith, H. 2016. Review of evolving trends in blended wing body aircraft design. *Progress in Aerospace Sciences* 82, 1–23.

[21] Okonkwo Chukwuemeka, P. P. and (Keine Angabe). 2016. *Conceptual Design Methodology for Blended Wing Body Aircraft*. PhD Thesis, Cranfield University.

[22] Prof. Dr.-Ing. Eike Stumpf. *UNICADO*. *Eine gemeinsame Flugzeugvorentwurfsumgebung der deutschen Luftfahrtuniversitäten*. https://www.dlr.de/pt-lf/desktopdefault.aspx/. Accessed 2 December 2023.

[23] Raymer, D. P. 1989. *Aircraft design*. *A conceptual approach*. AIAA Education Series. American Inst. of Aeronautics and Astronautics, Washington.

[24] Research in Flight. *Flightstream*. DARcorporation, Auburn, AL.

[25] Schneider, J. and Strohmayer, A. 2023. Development process for preliminary aircraft sizing methods with regard to new technologies. *AEAT* 95, 9, 1353–1362.

[26] Selig, M. *UIUC Airfoil Coordinates Database*. https://m-selig.ae.illinois.edu/ads/coord_database.html. Accessed 26 January 2024.

[27] Strohmayer, A. 2022. *Flugzeugentwurf I*. Vorlesungsskript, Stuttgart.

[28] van Dommelen, J. and Vos, R. 2014. Conceptual design and analysis of blended-wing-body aircraft. *Proceedings of the Institution of Mechanical Engineers, Part G: Journal of Aerospace Engineering* 228, 13, 2452–2474.

[29] Wikipedia. 2023. *Boeing B-47*. https://de.wikipedia.org/wiki/Boeing_B-47. Accessed 1 December 2023.

[30] Ye, Z. 2023. *Development of an Analytical Methodology for the Initial Sizing of Blended Wing Body Aircraft for the UNICADO Aircraft Design Software*. Universität Stuttgart, Stuttgart.

[31] Yu, G., LI, D., Shu, Y., and Zhang, Z. 2019. The Engine Position Effect on SWB Airplane Aerodynamic Performance. In *The Proceedings of the 2018 Asia-Pacific International Symposium on Aerospace Technology (APISAT 2018)*, X. Zhang, Ed. Lecture Notes in Electrical Engineering. Springer Singapore, Singapore, 201–210. DOI=10.1007/978-981-13-3305-7_16.